J Mater Sci (2008) 43:3223–3233
DOI 10.1007/s10853-008-2557-6

Comparison of failure mechanisms between rubber-modified and unmodified epoxy adhesives under mode II loading condition

Makoto Imanaka · Ryousuke Orita · Yosinobu Nakamura · Masaki Kimoto

Received: 30 October 2007 / Accepted: 13 February 2008 / Published online: 11 March 2008

Abstract The effect of rubber modification on fracture toughness of adhesive joints under mode II loading condition was investigated in comparison with that under mode I loading, wherein the two adhesives rubber-modified and unmodified were used. To evaluate the fracture toughness on the basis of *R*-curve characteristics under mode II loading condition, four-point bend tests had been conducted for the adhesively bonded end-notched flexure (ENF) specimens. Thus obtained *R*-curves revealed the following trend: its behavior did not appear for the unmodified adhesive, whereas the rubber-modified adhesive exhibited a typical behavior. In the initial stage of crack propagation, G_{IIC} of the rubber-modified adhesive is lower than that of the unmodified adhesive, but becomes greater in the range of $\Delta a > 25$ mm. Nevertheless, the significant improvement of the fracture toughness with the rubber modification under mode I loading condition was not observed under mode II loading. Moreover, FEM analysis was made to elucidate the relation between the above fracture behavior and stress distributions near the crack tip. The results gave the reasonable relationship between evolution of plastic zone and the area with high void-fraction as well as the *R*-curves behavior. In addition, macroscopic and SEM observations for the fracture surfaces were also conducted.

M. Imanaka (✉) · R. Orita
Department of Technology Education, Osaka University of Education, Kashiwara, Osaka 582-582, Japan
e-mail: imanaka@cc.osaka-kyoiku.ac.jp

Y. Nakamura
Department of Applied Chemistry, Osaka Institute of Technology, Osaka 535-8585, Japan

M. Kimoto
Department of Chemistry and Environment, Technical Research Institute of Osaka Prefecture, Osaka 594-1157, Japan

Introduction

Rubber-modified epoxy adhesives have attracted special interest from satisfying static strength and toughness simultaneously; numerous studies have been conducted on fracture toughness of several types of adhesive joints bonded with the rubber-modified adhesives, in special, under mode I loading condition [1–6]. In such situation, it is well known that the main improvement mechanism of the fracture toughness is shear banding in the epoxy matrix running among the rubber particles and plastic void growth initiated with cavitation or debonding of the rubber particles due to the high expansion stress in front of the crack tip [7]. Although adhesive joints are usually designed to minimize any applied mode I loading, there are little studies on fracture toughness under mode II loading condition [8–12]. Expansion stress under mode II loading is remarkably small in contrast with that under mode I loading; hence, both cavitation and debonding of the rubber particles are expected to be suppressed for lack of expansion stress. Thus it is necessary to clarify whether the rubber modification improves the fracture toughness under mode II loading or not. Unfortunately, there are few literatures concerned with the effect of rubber modification [13–15]. In the present situation, it is still unclear that the rubber modification improves the fracture toughness under mode II loading or not.

In this study, the effect of rubber modification on the fracture toughness of adhesive joints under mode II loading condition was investigated in comparison with

that under mode I loading, wherein four-point bend tests for adhesively bonded end-notched flexure (ENF) specimens were conducted to evaluate the fracture toughness on the basis of *R*-curve characteristics. To elucidate its modification effect, macroscopic and SEM observations for the fracture surfaces were also made together with stress whitening and void distribution. Furthermore elastic-plastic finite element analyses were carried out to obtain the stress and strain distributions near the crack tip, in which Gurson's model was applied for the rubber-modified adhesive to take the extension of void-fraction from rubber particles into account. Based on these results, the effect of rubber modification on the crack initiation and its propagation behavior was discussed.

Preparation of adhesives and mechanical properties

Two kinds of epoxy adhesives were used in the present study. One was a rubber-modified epoxy adhesive prepared from dispersing cross-linked rubber particles (XER-91, JSR) in bis-phenol epoxy resin (Epikote 828); the other was an unmodified epoxy adhesive without rubber particles. For both the adhesives, piperidine was used as a curing agent; the mix proportion of the adhesives and curing conditions are listed in Table 1.

To investigate the effect of rubber modification on the mechanical properties of the bulk adhesives, tensile tests were conducted by using dumbel (JIS.K7113) type specimens at the cross-head speed of 1 mm/min. Figure 1 shows stress–strain curves of the modified and unmodified adhesives, whose mechanical properties are summarized in Table 2. As Fig. 1 shows, both the adhesives clearly yield the behavior before the final fracture, also indicating that the rubber modification decreases both the Young's modulus and fracture stress, but increases the breaking strain dramatically.

Table 1 Preparation of the epoxy adhesives

	Composition		Curing condition
Rubber-modified adhesive	Epoxy resin	8.6 g	20 h at 393 K
	Rubber particles (XER-91[a])	1.4 g	
	Piperidine	0.43 g	
Unmodified adhesive	Epoxy resin	8.6 g	
	Piperidine	0.43 g	

XER-91[a]: cross-linked rubber particles
(Mean diameter 70 nm)

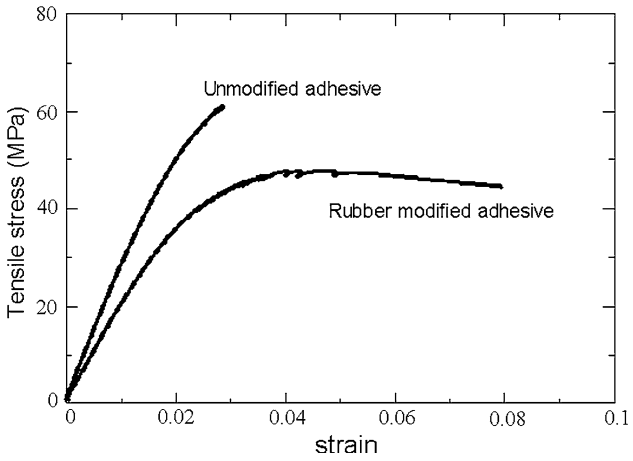

Fig. 1 Stress–strain curves of bulk adhesives

Experimental procedure of fracture toughness tests

Figure 2a and b shows the shape and sizes of the adhesively bonded end-notched flexure (ENF) and double cantilever beam specimens, respectively. The former specimen was used for fracture toughness tests under mode II loading, the latter for that under mode I loading. A tool steel (JIS.SKD11) and structural carbon steel (JIS S55C) were used as adherents for the ENF and DCB specimens, respectively. A filler gage of 0.01 mm in thickness, treated with a release agent, was used as a pre-crack between Teflon sheets of 0.1-mm thickness as in Fig. 2a. We adapted similar method to induce a pre-crack in the adhesive layer of the DCB specimen as in Fig. 2b.

Schematic illustration of four-point bend test for the ENF specimen is shown in Fig. 3. The load is introduced via steel ball onto a loading platen, allowing it to rotate freely, which ensures that the applied load on the right loading pin is equal to that on the left one. The bending test was conducted at the cross-head speed of 1 mm/min, then the deflection of the specimen being monitored on a clip gage inserted between the loading platen and base plate. To obtain *R*-curves, the crack extension was measured in several stages before failure in accordance with the following method. The specimen was rapidly unloaded before unstable crack propagation, the removed specimen being immersed in a solution of fluorescent to mark the cracked surface. The crack extension was measured from the fracture surface under UV light. The energy release rate was calculated in terms of the crack extension and the load just before unloading; the detail will be described later. Furthermore, to observe the behavior of the damage evolution, the crack tip region was monitored with the aid of high-magnified video camera during loading.

Table 2 Mechanical properties of the adhesives

	Young's modulus E (MPa)	Yield stress σ_y (MPa)	Work hardening parameter H (MPa)
Unmodified adhesive	2842.0	40.0	$0 < \varepsilon_p$:$H = 800$
Modified adhesive	1985.0	26.8	$0 < \varepsilon_p < 0.0154$:$H = 1110$
			$0.0154 < \varepsilon_p$:$H = 0$

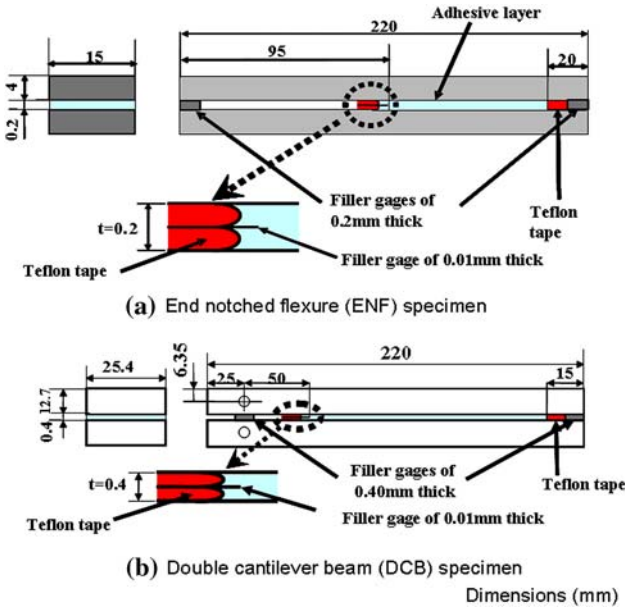

Fig. 2 Shape and sizes of the adhesively bonded ENF and DCB specimens

Tensile load under mode I loading condition was applied to the DCB specimen by use of a universal testing machine (Shimadzu Autograph, DCS-500), whereby the cross-head speed for loading is 1 mm/min. The displacement of the loading points was measured on a clip gage, crack extension being also measured by the same method as that under mode II loading.

Experimental results and discussion

Compliance calibration tests

Based on the beam model of the 4ENF specimen, the average displacement and compliance for the configuration illustrated in Fig. 3 [16] are given as Eqs. 1 and 2,

$$\delta_{\max} = \frac{\delta_1 + \delta_2}{2} = \frac{S_L^2}{8Ebh^3}(6L - 10S_L + 9a)P + \frac{3S_L P}{5Gbh} \quad (1)$$

$$C = \frac{\delta_{ave}}{P} = \frac{S_L^2}{8Ebh^3}(6L - 10S_L + 9a) + \frac{3S_L}{5Gbh} \quad (2)$$

where δ_1 and δ_2 represent the deflection of the specimen underneath the left and right loading pin, respectively. a is the crack length which is represented as the distance from crack tip to the left loading roller. b and h are the width and thickness of the adherent, respectively, E and G are Young's and shear moduli of the adherent, respectively. P is the applied load. The other symbols are defined in Fig. 3.

Equation 2 indicates a linear relationship between compliance and crack length. Figure 4a shows the experimental result for the ENF specimen together with a theoretical line based on Eq. 2. To prevent the influence of the loading rollers, the compliance was measured with crack tips greater than 15 mm away from the loading rollers. From the comparison of the experimental data and the theoretical line, it is found that the experimental data are significantly greater than the theoretical line. Similar trend had also been reported in 4ENF tests of laminated composites, wherein the cause of

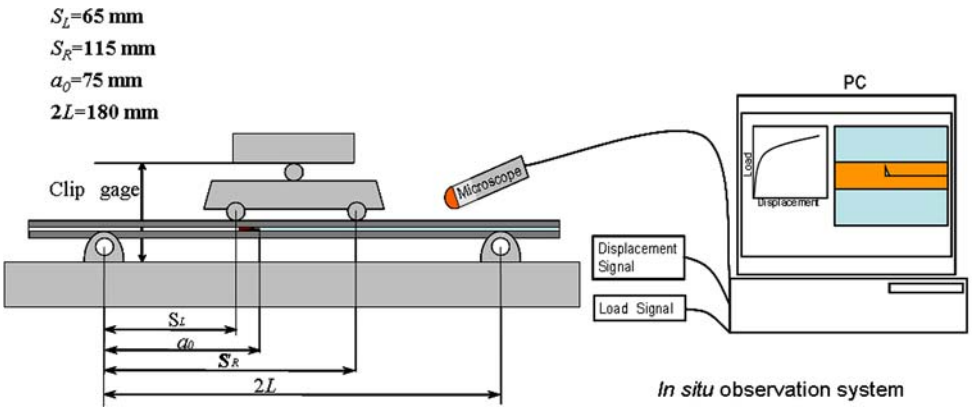

Fig. 3 Schematic illustration of ENF test

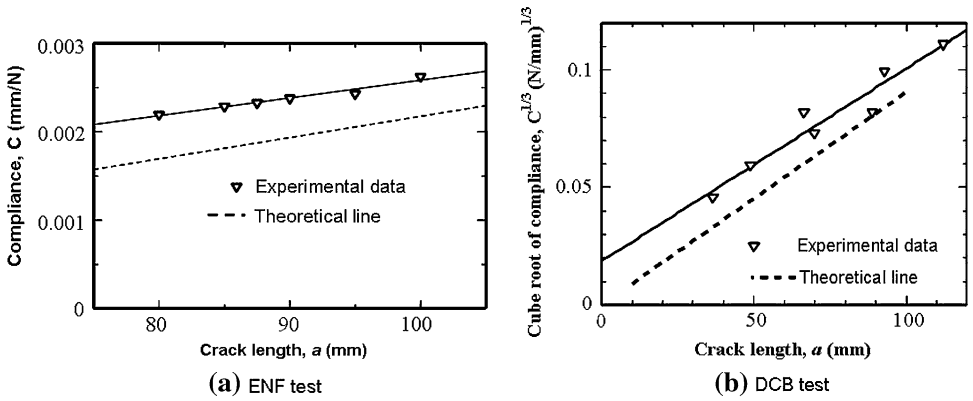

Fig. 4 Compliance as function of crack length

the difference was expected from neglecting the shear deformation in the specimen and deformations in the load train in the beam theory [17]. Thus the experimental results are represented as the following linear equation.

$$C = C_0 + C_1 a \tag{3}$$

where C_0 and C_1 are the constants calculated by the least square method, the slope of the experimental line being similar to that from the beam theory. Substituting Eq. 3 into the fundamental equation, we can obtain the energy release rate as follows:

$$G_{\mathrm{IIC}} = \frac{P^2}{2b}\frac{\mathrm{d}C}{\mathrm{d}a} = \frac{P^2}{2b}C_1 \tag{4}$$

Equation 4 indicates that the energy release rate is independent of the crack length and then linearly increases with the increase of C_1. Thus, from the slope of the experimental line the energy release rate can be evaluated. With regard to the evaluation of G_{IIC}, it is pointed out that the effect of friction on G_{IIC} value obtained from 4ENF test is larger than that from 3ENF test; however, it can be lowered with decreasing ratio of the inner span length to the outer one [18, 19]. For example, results of FEM analysis for 4ENF tests of laminated composites gave that the friction effect obtained at the span ratio of 0.4 greater than that obtained from 3ENF tests by a factor of about 4% [18]. In the present experiment, the span ratio is about 0.3; hence, the effect of friction could be expected to be negligible.

The result for the DCB specimen under mode I loading gives a relationship between the crack length, a, and cube root of compliance, $C^{1/3}$, as in Fig. 4b, which fits the following linear equation.

$$C^{1/3} = D_0 + D_1 a \tag{5}$$

Substituting Eq. 5 into the fundamental equation, we can obtain the energy release rate as follows:

$$G_{\mathrm{IC}} = \frac{P^2}{2b}\frac{\mathrm{d}C}{\mathrm{d}a} = \frac{3D_1 P^2 C^{2/3}}{2b} \tag{6}$$

Equation 6 is often used for evaluating energy release rate of adhesively bonded DCB specimens.

Load–displacement curves

Figure 5a and b shows load–displacement curves for the ENF specimens with unmodified and rubber-modified adhesives, in which video micrographs near the crack tips are also given at several load levels. As Fig. 5a and b shows, a linear relationship is maintained just before a peak value for the unmodified adhesive, whereas load–

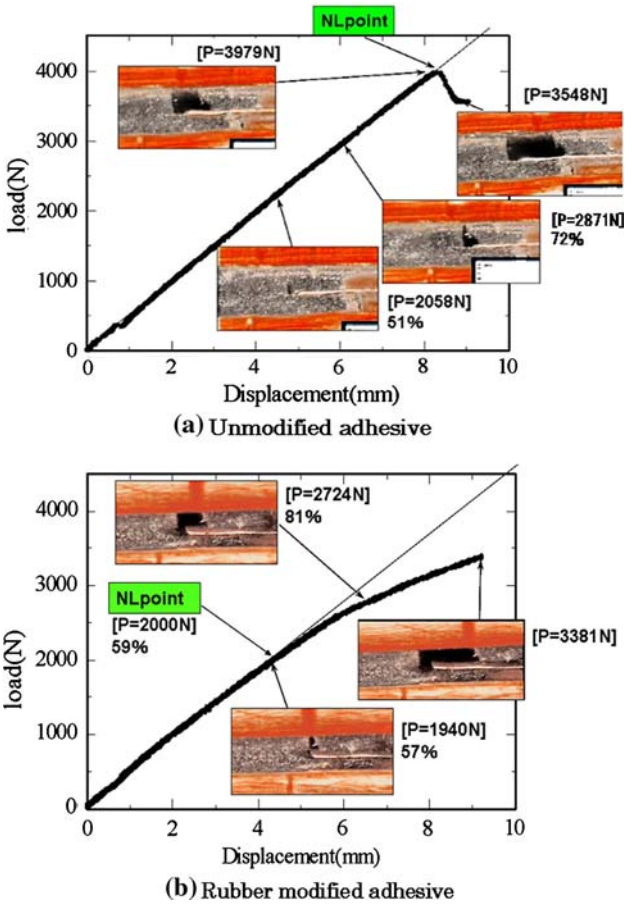

Fig. 5 Load–displacement curves for ENF specimens with rubber-modified and unmodified adhesives, wherein video microphotographs of the fracture process are included

displacement curve for the modified adhesive deviates from linear line at about 60% of the peak value. Besides, such a point at which the load–displacement curve deviates from linear line is illustrated as NL point in Fig. 5, where crack propagation occurs above the NL point [11].

For the unmodified adhesive, triangle void appears in front of the pre-crack at the load of 60% of the NL point as in Fig. 5a, the void expands to the upper interface, and begins to contact with the interface at the load of 72% of the NL point; subsequently, the interfacial crack appears at the contact point and propagates rapidly in the vicinity of the NL point. When the void proceeded to the upper interface, the void periphery forms wedge shape at the contact point. The stress singularity of the wedge tip is weaker than that at the crack tip, which can induce the stress blunting. This may be a reason why there is a considerable increase in the load for duration from the arrival of the void onto the upper interface to the propagation of the interfacial crack. Thus the load reaches a steady-state value through a rapid decrease.

For the modified adhesive, on the other hand, the void reaches the upper interface near the NL point as in Fig. 5b, so that crack propagates immediately after reaching the upper interface. The inset micrographs indicate that the void appears in front of pre-crack and propagates to the upper interface; subsequently, the crack propagates along the interface for both the adhesives. Such a fracture process is schematically illustrated in Fig. 6. Chain et al. also reported similar failure process for adhesively bonded ENF specimen under three-point bending condition: the central crack shifts to the upper interface (compression side), whereby void appeared in front of the pre-crack, as shown in Fig. 6 [12]. Such a behavior of crack propagation agrees with that expected from contour and vector plots of the maximum principal stress obtained by FEM analysis, as will be discussed in the later section. For some adhesives, it is reported that micro-cracks be observed in front of the pre-crack under mode II loading condition [11]; however, such micro-cracks were not observed for the present adhesives.

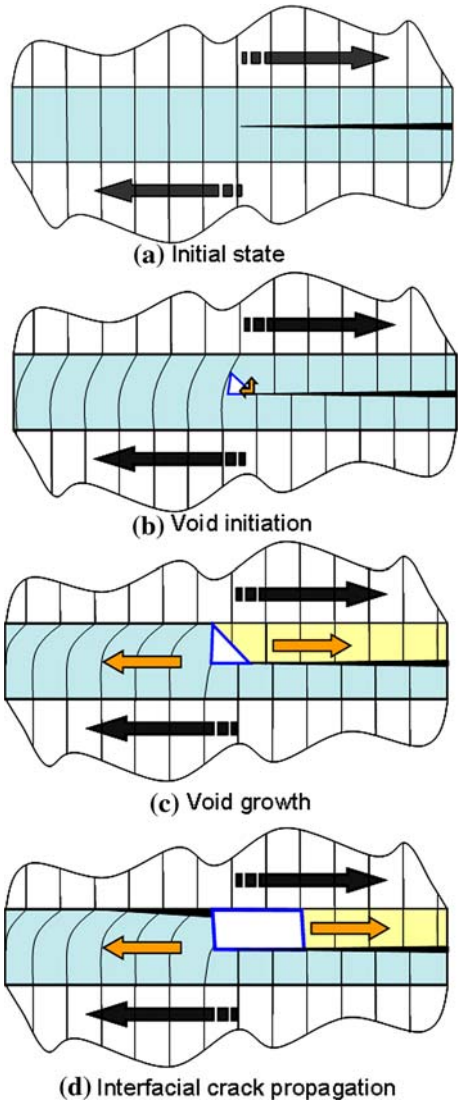

Fig. 6 Illustration of fracture process of the ENF specimen

R-curves

Figure 7 shows the *R*-curves of the ENF specimens with rubber-modified and unmodified adhesives, wherein two load displacement curves near the peak points for the unmodified one are also given. As the inset figure shows, the curves reach a steady-state values. In the 4-ENF test, G_{IIC} depends only on the applied load from Eq. 4. This means that the crack propagates at a constant energy release rate in the steady-state region. Thus, *R*-curve

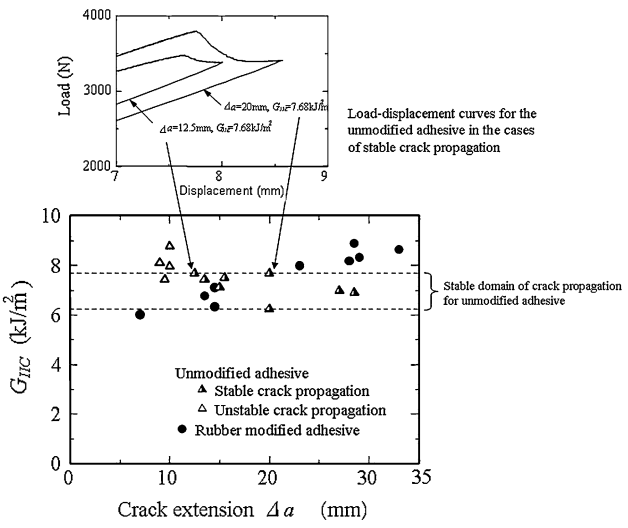

Fig. 7 *R*-curves under mode II loading

behavior does not appear for the unmodified adhesive, and the transitional G_{IIC} values before reaching steady state are considered to be extrinsic toughness. The G_{IIC} values in the steady-state region ranges from 6.2 to 7.7 kJ/m^2 as in Fig. 7.

In contrast to the unmodified adhesive, G_{IIC} of the rubber-modified adhesive increases with crack growth in the whole range of the growth, that is a typical behavior of *R*-curve. Hence, in the initial stage of the crack propagation, G_{IIC} of the modified adhesive is lower than that of the unmodified one, but becomes greater in the range of $\Delta a > 25$ mm.

Kim et al. reported that fracture toughness of epoxy adhesive was decreased with the rubber modification under mode II loading condition [13]. Their result was evaluated for adhesively bonded compact shear (CS) specimens; thus, it can be expected that the fracture toughness of the CS specimens corresponds to the energy release rate of the ENF specimen in the initial stage of crack propagation. This implies that the energy release rate decreases in the initial stage with the rubber modification, which agrees with the trend of G_{IIC} in Fig. 7 as mentioned above.

Contrary to the results, Ookubo et al. gave that the rubber modification increased the fracture toughness under mode II loading in different epoxy system, whereby adhesively bonded tapered ENF specimens were used under bending load condition [15]. Although the crack propagated gradually for the tapered ENF specimen in a trend similar to the present four-point bending ENF test, they calculated the critical energy release rate based on the peak load without taking crack growth into consideration.

Applying to the above evaluation method based on the peak load for the present adhesives, the critical energy release rates obtained for the unmodified and modified adhesives correspond to the value of G_{IIC} in the initial and finial stages of the crack propagation, respectively: the critical energy release rates from the peak load for the unmodified adhesive range from 7.5 to 9.5 kJ/m^2, which is nearly equal to G_{IIC} for modified one (see Figs. 6 and 7). Hence, the above two trends of fracture toughness do not conflict with that in this adhesive system.

Figure 8 shows *R*-curves of DCB specimens with the modified and unmodified adhesives under the mode I loading. With a rubber modification a dramatic improvement of fracture toughness is also observed for bulk DCB specimens with the same epoxy resin and curing agent used to the present adhesive [20]. In the figure, G_{IC} is found to be improved over ten times with the rubber modification. This indicates that the rubber-modification effect on the fracture toughness under mode II loading be small compared to that under mode I loading.

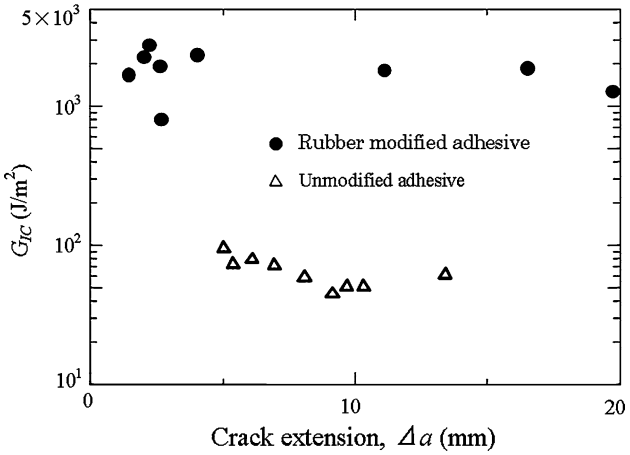

Fig. 8 *R*-curves under mode I loading

Fracture surface observation

Figure 9 is an example of the macroscopic and SEM photos of fracture surfaces of the DCB specimen bonded with the rubber-modified adhesive, wherein stress

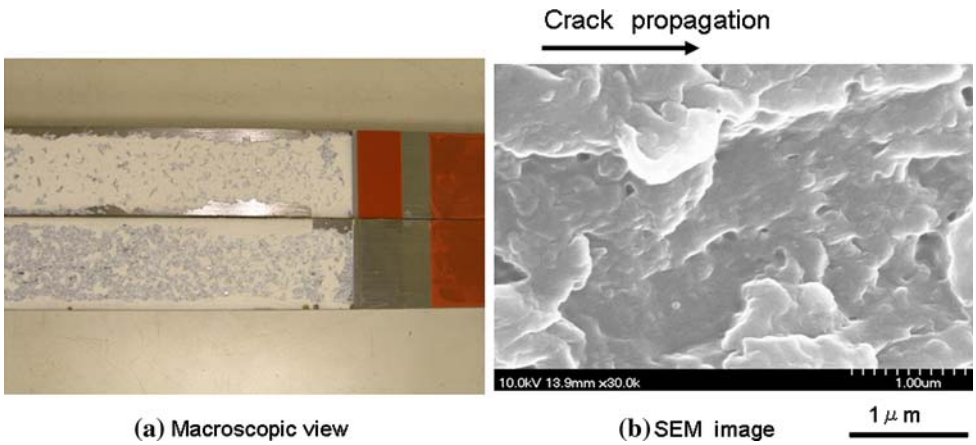

Fig. 9 Fracture surfaces of DCB specimen

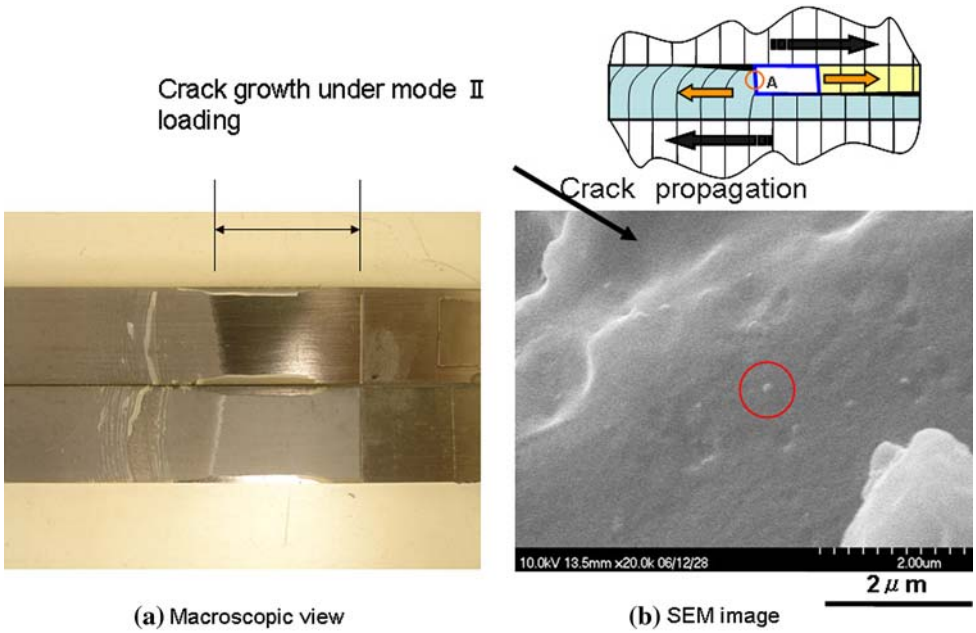

Fig. 10 Fracture surfaces of ENF specimen

whitening is also observed on the whole surface of the DCB specimen having cohesive fracture pattern in Fig. 9a. The stress whitening of rubber-modified epoxy resin under mode I loading condition is, in general, considered to be a formation of a damage zone induced from the cavitation or debonding of rubber particles due to the expansion stress [21]. Figure 9b indicates that numerous holes are formed and then fracture surface is severely deformed as a typical fracture surface of rubber-modified adhesive.

Fracture surfaces of ENF specimen bonded with the rubber-modified adhesive are shown in Fig. 10. In contrast to the DCB specimen, interfacial fracture is observed in the region of mode II crack propagation as in Fig. 10a. Kim et al. also reported interfacial fracture under mode II loading condition for the CS specimens bonded with rubber-modified epoxy adhesive mentioned above [13]. Figure 10b represents SEM observation in the cohesive fracture area near the pre-crack, indicating that the fracture surface is flat and there are few holes as trace of debonded rubber particles. This implies that the debonding can be suppressed for lack of expansion stress under mode II loading.

Stress analysis

Both characteristics of the crack locus and *R*-curve are related to the stress conditions near the crack tip. Here we made FEM analysis for the ENF specimens in two cases: one is before crack propagation through the crack tip located in the middle of the adhesive layer, and the other is for crack propagation process in the tip located at the upper adhesive/adherent interface. The FEM program code used in this analysis was of MSC-MARC. Figure 11 shows the boundary conditions for the ENF specimen. This analysis was performed under the assumption of plane strain condition, incremental loads being applied to the upper loading pins. To prevent overlap of the crack face, its contact was constricted by using contact elements illustrated in Fig. 11, where the coefficient of friction was considered to be zero. In addition, the adherent was treated as an elastic material whose Young's modulus and Poisson's ratio are 205.8 GPa and 0.33, respectively. The unmodified adhesive was treated as an elastic–plastic material having material constants listed in Table 2, whereas Gurson's model was applied to the modified adhesive, because of proceeding in yielding behavior due to the voids formation from rubber particles. Details of Gurson's model will be described later.

At first, the relation between the crack locus and stress distributions around the crack tip was discussed. As mentioned previously, for both the rubber-modified and unmodified adhesives, the void appears in front of the crack tip and propagates in the direction of the upper interface. Crack is, in general, liable to propagate in the perpendicular direction of the maximum principal stress. Thus, the stress was analyzed for the unmodified adhesive because its crack propagation locus is similar to that for the modified adhesive.

Figure 12a and b shows the vector and contour plots of the maximum principal stress, respectively, where the crack tip is located in the middle of the adhesive layer. As Fig. 12a shows, the direction of the maximum stress near crack tip indicates that there are two possibilities in the direction of crack propagation: one is of the upper and the

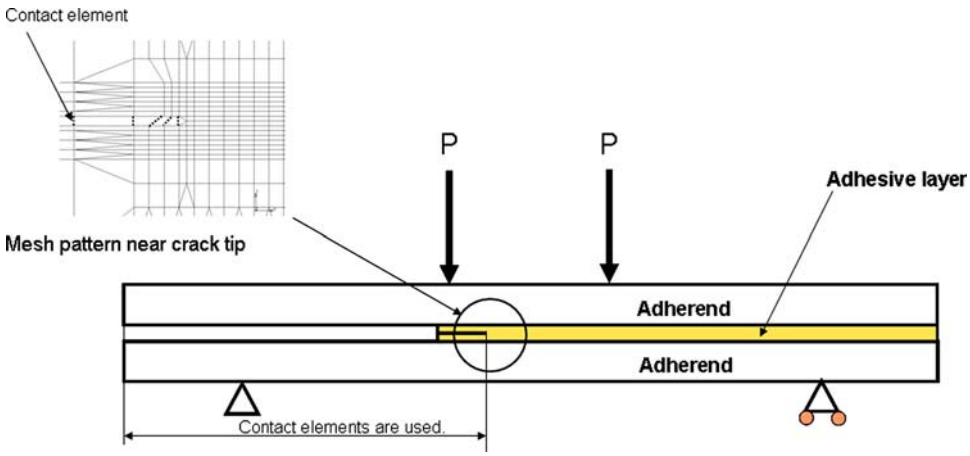

Fig. 11 Boundary conditions for ENF specimen under mode II loading

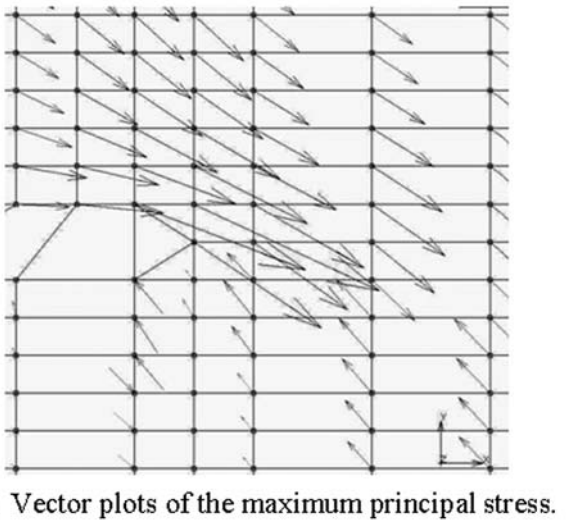

Fig. 12 The maximum principal stress near pre-crack tip ($G = 6{,}548$ J/m^2)

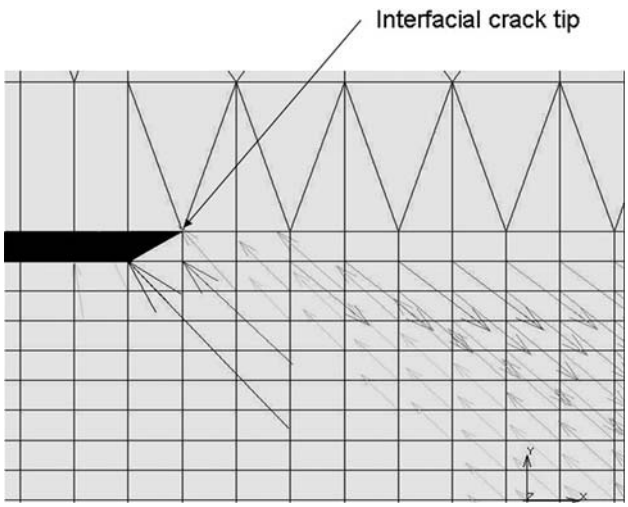

Fig. 13 Vector plots of the maximum principal stress near interfacial crack tip ($G = 6{,}548$ J/m^2)

other is of the lower interfaces. Figure 12b indicates that the maximum principal stress is concentrated at the upper cracked surface and the area subjected to high stress extends in the upper direction in the vicinity of the crack tip. Hence, the crack is expected to propagate in the upper direction that agrees with the experimental results in the previous section.

Figure 13 shows the vector plots of the maximum principal stress in the process of crack propagation, wherein the crack tip locates at the upper interface. The crack is expected to propagate through the upper adhered in the direction of the maximum principal stress; however, the crack could not penetrate into the adherent, so that it propagates along the interface. Such a trend is also in agreement with the experimental results.

Subsequently, the relation between stress distributions and *R*-curve characteristics was discussed. The extent of plastic and damage zones near the crack tip is related in

terms of the crack initiation and propagation characteristic. To investigate the effect of rubber modification on the extent of the plastic and damage zones, the evolution of the two zones was analyzed for both the adhesives. As described above, the unmodified and modified adhesives are treated as elastic-plastic and Gurson's materials, respectively. For the rubber-modified polymers, the understanding of micro-mechanics has greatly advanced through numerical works [22–24]; however, the criteria of yield condition and damage evolution for the rubber-modified polymers have not been formulated for the use of FEM analysis.

The approximate constitutive equation proposed by Gurson is widely available for estimating yielding behavior of ductile materials [25, 26], that is an only method for simulating the yield and damage zones by use of FEM analysis in the present situation. Furthermore, Gurson's constitutive equations were applied to calculation of the yield stress and shape of damage zone around the crack tip for rubber-modified epoxy resins, where rubber particles were considered to act as the initial voids [27–29]. In the present study, the rubber-modified adhesive was treated as a Gurson's material, the following modified Gurson's constitutive equation being applied for the adhesive layer.

$$F = \left(\frac{\sigma_M}{\sigma_y}\right)^2 + 2q_1 f \cosh\left(\frac{q_2\sigma_{kk}}{2\sigma_y}\right) - \{1 - (q_1 f)^2\} = 0 \tag{7}$$

where F is the yield function, σ_y the yield stress of matrix, σ_{kk} the first stress invariant, f the void-volume fraction, σ_M the Mises equivalent stress, and q_1 and q_2 the yield surface multipliers. In the present work, the rubber particles were assumed as initial voids, the coalescence and nucleation of voids being neglected, and that the matrix was plastically incompressible. Hence, the change in the void-volume fraction during an increment of deformation can be given by

$$\dot{f} = (1-f)\dot{\varepsilon}^p_{kk} \tag{8}$$

where $\dot{\varepsilon}^p_{kk}$ is the increment of hydrostatic strain of the plastics, and $\dot{f}$ is the increment of the void-volume fraction.

In application of Gurson's model to the adhesive layer, material constants of the bulk resin, the initial void-fraction, and the surface multipliers, q_1 and q_2, are required, which are given as follows: material constants of the bulk matrix resin are the same as those of the unmodified adhesive listed in Table 2, the initial void-fraction is 0.14, $q_1 = 1.0$ and $q_2 = 1.9$. Similar to the stress analysis for the maximum principal stress, both the plastic and damage zones were analyzed in two cases: the crack tip locates in the middle of the adhesive layer and at the interface.

Figure 14 shows contour plots of plastic strain, ε_p, and void-fraction, f, near the crack tip located at the adhesive/adherent interface. In Fig. 14a, b, the size of plastic zone expands in front of the interfacial crack tip for both the adhesives, where the size of plastic zone with the strain of $\varepsilon_p > 0.12$ for the modified adhesive is so large as three times for the unmodified one. This indicates that the rubber modification enlarges the plastic zone. Figure 14c shows that the void-fraction increases not only in the vicinity of the crack tip but also away from the crack tip, though being restricted within shallow area from the interface. The increase in the void-fraction promotes the expansion of the plastic zone. This may be a reason why the plastic zone of the rubber-modified adhesive is larger than that of the unmodified one. Thus, it is expected that more energy is dissipated with the plastic deformation through the rubber modification. Since the total energy release rate is the same for the each adhesive, the remaining energy used for crack propagation decreases with the rubber modification. This

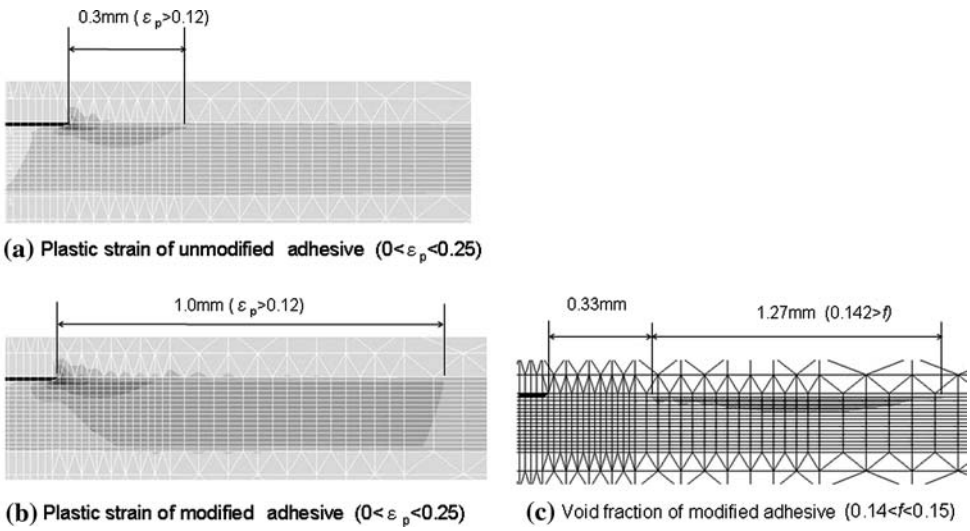

Fig. 14 Contour plots of plastic strain and void-fraction near interfacial crack tip (G = 6,548 J/m^2)

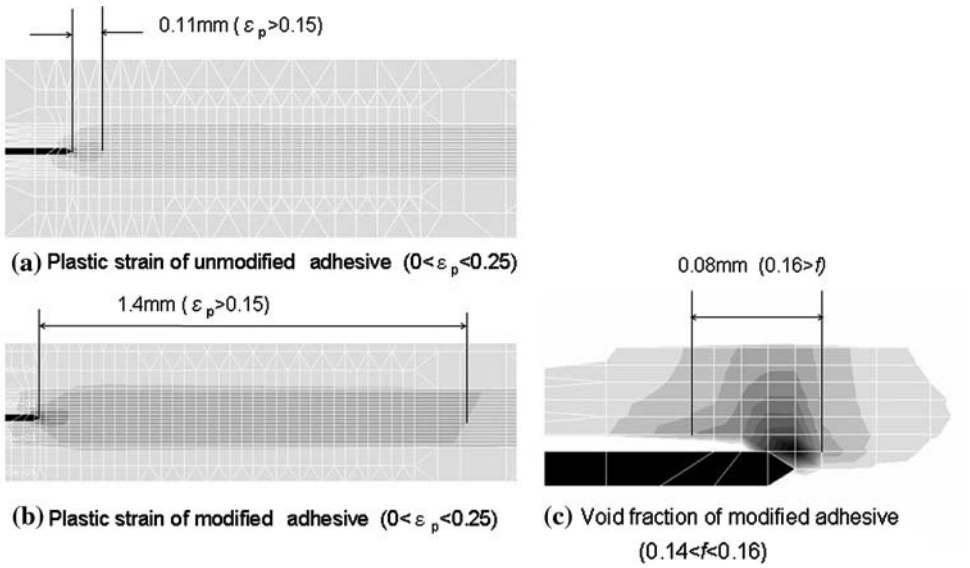

Fig. 15 Contour plots of plastic strain and void-fraction near pre-crack tip (G = 6,548 J/m^2)

agrees with the trend of R-curves in Fig. 8: in other words, the crack resistance is increased with the rubber modification.

For the crack tip located in the middle of the adhesive layer, contour plots of plastic strain and void-fractions are shown in Fig. 15. The size of plastic zone with the strain of $\varepsilon_p > 0.15$ also increases through the rubber modification as in Fig. 15a and b. In contrast to the interfacial crack with increasing void-fraction in wide range as in Fig. 14c, void-fraction of the rubber-modified adhesive increases in extremely localized area in Fig. 15c. This indicates that the increase in the void-fraction does not promote the expansion of the plastic zone. Usually, the increase in void-fraction enlarges the plastic zone but decreases the cohesive strength. In Fig. 5, the localized zone is almost the same in area as the triangle at the void initiation, which may be act as a trigger of the crack initiation. This may be one reason why G_{IIC} for the rubber-modified adhesive is less than that for the unmodified one in the initial stage of the crack propagation as in Fig. 7.

Conclusions

The effect of rubber modification on fracture toughness of adhesive joints under mode II loading condition was investigated in comparison with that under mode I loading condition. To observe the crack growth behavior under mode II loading, four-point bend tests were conducted for the adhesively bonded end-notched flexure (ENF) specimens. Moreover, FEM analysis was made to elucidate the relation between the fracture behavior and stress distributions near the crack tip. The summary is as follows:

(1) Under mode II loading condition, the void appeared in front of the crack tip and propagated in the direction of the upper interface for both the adhesives. For the rubber-modified adhesive, the crack propagated along the adhesive/adherent interface at about 60% of the peak load, whereas for the unmodified adhesive it did just before fracture.

(2) The crack resistance for the unmodified adhesive did not increase with crack length, whereas R-curve behavior was found for the rubber-modified adhesive. Hence, in the initial stage of the crack propagation, G_{IIC} for the rubber-modified adhesive is lower than that of the unmodified adhesive, but becomes greater in the range of $\Delta a > 25$ mm. In contrast to the fracture toughness under mode I loading, G_{IC} was improved over ten times by the rubber modification. It can be concluded that the effect of rubber modification on the fracture toughness under mode II loading is small compared to that under mode I loading.

(3) The degree of stress whitening for the ENF specimen with the rubber-modified adhesive was not so clear in comparison with that for the DCB specimen. SEM observation showed that trace of debonded rubber particles formed itself into many holes and fracture surface is deformed severely for the DCB specimens, whereas for the ENF specimen, the fracture surface was flat and there were few holes.

(4) FEM analysis in two different locations near the crack tip gave that an increase in the plastic zone with the rubber modification reasonably coincided with the trend of R-curves corresponding to the increase in the crack resistance. In view of the void-fraction behavior, we gave a reason why G_{IIC} in the

initial stage of the crack propagation for the rubber-modified adhesive is less than that in the unmodified one.

Acknowledgements The Authors would like to acknowledge Japan Synthesis Rubber Co. for Providing XER-91.

References

1. Bascom WD, Cottington RL, Jones RL, Peyser P (1975) J Appl Polym Sci 19:2524
2. Bascom WD, Cottington RL (1976) J Adhes 7:333
3. Rakestraw MD, Taylor NW, Dillard AD, Chang T (1995) J Adhes 55:123
4. Daghyani HR, Ye L, Mai Y-W (1995) J Adhes 53:149
5. Daghyani HR, Ye L, Mai Y-W (1996) J Mater Sci 31:2523. doi:10.1007/BF00687277
6. Ashcroft IA, Hughes DJ, Shaw SJ (2001) Int J Adhes Adhes 21:87
7. Yee AF, Person RA (1988) In: Roulin-Moloney AC (ed) Fractography and failure mechanism of polymers and composites. Elesvier Applied Science Publisher, London & New York, p 219
8. Chai H (1992) Int J Frac 58:223
9. Chai H (1998) Int J Frac 37:137
10. Daghyani HR, Ye L, Mai Y-W (1996) J Adhes 56:71
11. Blackman BRK, Kinloch AJ, Paraschi M (2005) Eng Frac Mech 72:877
12. Chai H, Martin YMC (1996) J Mech Phys Solids 44:1669
13. Kim HS, Ma P (1998) Key Eng Mater 137:179
14. Kim HS, Ma P (1998) J Appl Polym Sci 69:405
15. Ookubo K, Yoshimitu H, Fujii Y (2001) Trans JSME Ser A 67:106 (in Japanese)
16. de Morais AB, de Moura MFSF (2006) Eng Frac Mech 73:2264
17. Martin RH, Davidson BD (1999) Plast Rubber Comp 28:401
18. Schuecker C, Davidson BD (2000) ASTM STP 1383:334
19. Sun X, Davidson BD (2005) Int J Frac 135:51
20. Du J, Thouless MD, Yee AF (2000) Acta Mater 48:3581
21. Person RA, Yee AF (1989) J Mater Sci 24:2571. doi:10.1007/BF01174528
22. Guild FJ, Kinloch AJ (1995) J Mater Sci 30:1689. doi:10.1007/BF00351597
23. Chen XH, Mai Y-W (1998) J Mater Sci 33:3529. doi:10.1023/A:1004686708639
24. Chen XH, Mai Y-W (1999) J Mater Sci 34:2139. doi:10.1023/A:1004576213379
25. Gurson AL (1977) J Eng Mater Tech 99:2
26. Tvergaard V (1982) J Mech Phys Solids 30:399
27. Kody RS, Lesser AJ (1999) Polym Comp 20:250
28. Ikeda T, Mano J, Ikemoto D, Lee DB, Miyazaki N (2003) Trans Japan Soc Mech Eng 69:434 (in Japanese)
29. Imanaka M, Nakamura Y, Nishimura A, Iida T (2003) Comp Sci Tech 63:41